

Entrainment of Mutually Synchronized Spatially Distributed 24 GHz Oscillators

Christian Hoyer¹, Lucas Wetzel¹, Dimitrios Prousalis¹, Jens Wagner¹, Frank Jülicher¹,
and Frank Ellinger¹, *Senior Member, IEEE*

Abstract—Synchronization is one of the most challenging aspects of distributed systems in terms of their scalability. Minimal uncertainties can lead to problems or failures regarding data consistency in globally operating data centers or in distributed sensor arrays. Existing approaches to address these challenges are based on hierarchical synchronization concepts which are well understood and have reached technical maturity, but have the disadvantage of having a single point of failure. However, especially for critical infrastructure or backup more resilient solutions are required. Mutual synchronization where oscillators in a network are coupled bidirectionally without a reference have been considered. Due to the flat hierarchy such systems do not have a single point of failure. This work studies how hierarchical synchronization can be combined with architectures implementing mutual synchronization. A network of three mutually coupled 24 GHz oscillators is used to study how injecting a reference signal into one oscillator affects the dynamics. This can be quantified by analyzing in which range of frequencies the network of mutually coupled oscillators can follow the reference frequency. Measurements on a ring and chain network topology forced by an external reference oscillator shown here are in good agreement with the predictions of a nonlinear dynamical model.

Index Terms—Delays, phase noise, frequency synchronization, frequency measurement, phase locked loops, propagation delay, communication systems, stability criteria, synchronization, mutual synchronization, oscillator.

I. INTRODUCTION

SINCE the 1960s, the synchronization of distributed locations has been an important challenge in the implementation of many technical systems. For example, the potential for synchronization of pulse coded modulation in telephone networks [1], [2], [3], [4], [5], [6], [7], [8] or early digital communication networks [9], [10], [11] was discussed thoroughly.

Manuscript received 12 December 2022; revised 27 February 2023; accepted 1 April 2023. This work was supported by the Federal Ministry of Education and Research (BMBF) under Grant 03VP06432 and as part of Germany's Excellence Strategy—EXC 2050/1—Project ID 390696704 — Cluster of Excellence “Center for Tactile Internet with Human-in-the-Loop” (CeTI) of Technische Universität Dresden. This article was recommended by Associate Editor H. Sjoland. (*Corresponding author: Christian Hoyer.*)

Christian Hoyer is with the Chair for Circuit Design and Network Theory, Technische Universität Dresden, 01069 Dresden, Germany (e-mail: christian.hoyer1@tu-dresden.de).

Lucas Wetzel, Dimitrios Prousalis, and Frank Jülicher are with the Max Planck Institute for the Physics of Complex Systems, 01187 Dresden, Germany (e-mail: lwetzel@pks.mpg.de).

Jens Wagner and Frank Ellinger are with the Centre for Tactile Internet with Human-in-the-Loop (CeTI) and the Chair for Circuit Design and Network Theory, Technische Universität Dresden, 01069 Dresden, Germany.

Color versions of one or more figures in this article are available at <https://doi.org/10.1109/TCSI.2023.3264996>.

Digital Object Identifier 10.1109/TCSI.2023.3264996

In this context, phase averaging has become a popular method for synchronization. Each node receives signals dedicated to synchronization from other nodes, averages their phases, compares the result with the phase of the local oscillator and adjusts its frequency according to predefined rules [1], [2], [3].

This concept is referred to as mutual synchronization and synchronized states can emerge through self-organized dynamics. In such systems, network synchronization is unaffected by the failure of individual nodes and perturbations to synchronized states decay within the boundaries of their basin stability [8], [9], [12]. In addition, the network can achieve synchronization at an optimal operating point for all nodes [13]. However, this depends on the characteristics of the network and in particular the time delays between coupled nodes [12], [14], [15], [16].

Another commonly used concept for synchronization is hierarchical primary-secondary synchronization. This approach is a very simple, straightforward concept [14], [17]. A signal derived from a precise primary reference clock is distributed directly or indirectly to at least one secondary oscillator via a clock tree. In this way, very tight control of all clocks can be ensured. This approach leads to frequency synchronization with the primary clock and is stable by definition. Thus this approach is used in many existing systems [18], [19], [20], [21]. Note that transmission time delays between the primary and secondary clock do not affect the stability of synchronization but introduce phase-differences [22].

The research presented here investigates the combination of these synchronization concepts to achieve a robust and easy-to-implement synchronization layer. For many spatially distributed applications, such as sensor networks, financial transactions, or globally distributed data centers, a reliable time reference is necessary to allow for robust data processing [23], [24], [25], [26]. For example, when accessing data in data centers, an uncertainty in clock synchronization of only 10 μ s can lead to failures [26]. For such large systems, the complexity of implementing a synchronization layer that relies entirely on mutual coupling is challenging. Hence, it may be more efficient to combine established hierarchical concepts with mutually coupled topologies [12], [27]. The stability of such hybrid concepts has been investigated in simulation, e.g. in a network of unidirectional coupled nodes in a ring arrangement [28], [29].

Similar structures, where a fixed reference is used to entrain a network of coupled oscillators can be found in system-on-chip architectures for distributed clock generation [30]. Due to the increasing integration of synchronous digital circuits,

the clock distribution remains a key challenge. Approaches to address them can be found in globally asynchronous, locally synchronous (GALS) synchronization schemes or in networks of coupled phase-locked loops (PLLs). In GALS, individual blocks are decoupled by asynchronous connections between clock domains, while coupled PLLs are used to achieve global synchronization between them [31], [32], [33]. However, due to the small physical distances within integrated circuits, delays between individual clocks are negligible or compensated, so that they have no significant impact on the coupling dynamics. The research presented here considers significant time delays of the order of the intrinsic periods of the oscillators and larger which cannot be neglected.

To gain a better understanding of the concept of mutual synchronization in the presence of cross-coupling time delays, Section II provides details about the dynamical model and existing phase-locked synchronized states in case of mutual coupling and entrainment. Due to the mutual coupling, particular focus is given to the limits of stability, which are different compared to the conventional PLL literature. In Section III, the design of a PLL node used for mutual coupling, as well as the measurement setup are presented. The results for mutual coupling with and without entrainment are shown and discussed in Section IV.

II. MODEL OF COUPLED OSCILLATORS

In [7] a linear model for mutual synchronization of an arbitrary number of geographically separated oscillators was presented and studied for zero time delays between individual nodes. However, no specific statement is made about the characteristics of the phase or frequency detection used. Reference [34] studies the dynamics and derives stability conditions for this linear model with delays between individual nodes. In [35] the analysis was extended to include component nonlinearities. An approach using feedback time delays to eliminate the dependence of the stability of synchronized states on the cross-coupling time delay has been proposed introducing the equational timing system (ETS) in [36]. However its dynamical response is more complicated and can not be solved analytically [36].

Theoretical studies of the probability density of the phase error for two mutually coupled oscillators using the Fokker-Plank equation are given in [37]. This analysis is continued in terms of the stochastic behavior of the oscillator's phase in [38] and [39]. Initial analysis of the hold-in and lock-in range of two coupled PLL systems are shown in [40]. There, a critical detuning is identified, for which a bifurcation to chaotic dynamics takes place. This is further elucidated in [41] and [42], defining the limit of synchronization for two coupled oscillators. In [43] and [44], the phase noise of an array of coupled oscillators is studied experimentally.

In recent years, the number of theoretical studies on mutual synchronization of oscillators has increased significantly, providing new insights into the complex dynamics of networks with time-delayed, nonlinear interactions [45], [46], [47], [48], [49]. Particularly, the analysis of networks of coupled PLLs has received increasing attention, resulting in theoretical frameworks for modeling such networks including

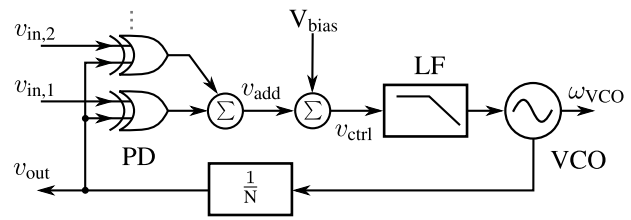


Fig. 1. Block diagram of the PLL node for mutual synchronization. Two of the in- and output channels are used, other unused channels are disabled and indicated by gray dots.

their complete nonlinear coupling characteristics [16], [52], [50], [51].

The dynamical model of one PLL node for mutual synchronization presented here is based on the simplified block diagram shown in Fig. 1. This block diagram consists of several phase detectors (PDs) that compare the phase of the PLLs output signal v_{out} to those of other connected PLL nodes, denoted by $v_{in,i}$, where i numbers the PDs. The output signals of the PDs are then summed to v_{add} and shifted by a constant calibration voltage V_{bias} . This is used to compensate for possible component heterogeneities and to tune the phase differences of a synchronized state. Subsequently, filtering is realized using a loop filter (LF). The resulting filtered signal tunes the voltage controlled oscillator (VCO). The frequency-divided oscillator signal serves as the output signal and reference signal for the phase detectors. Since the output signal is the input signal to all other connected nodes, the *reference* of a single node can be interpreted as the average frequency of all incoming signals in comparison to a conventional hierarchical concept [13], [15], [17].

In the following sections, the basic dynamical model of coupled PLL nodes is discussed. Here, the nonlinear nature of the oscillator is taken into account. Based on this theoretical framework, the procedure for determining the existence of possible mutually synchronized states is given. Subsequently, the entrainment of networks in ring and chain topologies consisting of three coupled PLLs is studied. In particular, the range in which the network mutually coupled oscillators can follow and lock to a reference signal, originated from a primary clock, is addressed.

A. Dynamical Model

The instantaneous output frequency $\dot{\phi}(t)$ of the VCO is a function of its nonlinear frequency response $g(\cdot)$, which is a function of the tuning voltage $v_{tune}(t)$

$$\omega_{VCO}(t) = \dot{\phi}(t) = g(v_{tune}(t)). \quad (1)$$

The characteristics of the frequency response $g(\cdot)$ depend on the topology of the oscillator which is defined in [53]. A functional representation is shown in [54]. The tuning voltage $v_{tune}(t)$ represents the control voltage v_{ctrl} which is filtered by the loop filter with impulse response $p(u)$. The control voltage v_{ctrl} consists of a constant calibration voltage V_{bias} as well as the weighted sum $v_{add}(t)$ of all phase detector

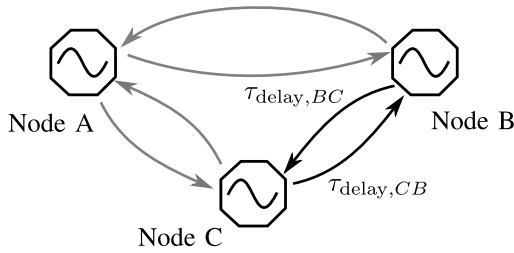


Fig. 2. Representation of a network of three mutually coupled PLL nodes in ring topology. As an example, the propagation time delays between the nodes C and B are given for this connection.

output voltages

$$v_{\text{tune}}(t) = \int_0^{\infty} p(u) \underbrace{(V_{\text{bias}} + v_{\text{add}}(t-u))}_{=v_{\text{ctrl}}(t-u)} du. \quad (2)$$

For each PLL k in the network, $v_{\text{add}}(t)$ is the weighted sum over its external inputs, equal to the number of PDs,

$$v_{\text{add}}(t) = \frac{1}{E_k} \sum_{i=1}^M d_{ki} v_{\text{in},i}(t) \oplus v_{\text{out}}(t). \quad (3)$$

Here, E_k denotes the number of oscillators connected to node k , M the total number of oscillators in the network, $v_{\text{out}}(t)$ is the feedback and output signal and $v_{\text{in},i}(t)$ corresponds to the external input signal to the phase detector from input i . This input is the time-delayed output of PLL i in the network. The phase detector performs an XOR operation, denoted by \oplus . The frequency of the output signal $v_{\text{out}}(t)$ is equivalent to the VCO frequency $\omega_{\text{VCO}}(t)$ divided by the frequency division factor N . The coupling parameter d_{ki} is either zero or one depending on whether there is a connection between node k and i , respectively.

B. Synchronized States in Mutually Coupled Oscillators

A network of three mutually coupled PLL nodes is studied to address the effects of open and periodic boundary conditions. Fig. 2 shows an example of a ring topology with periodic boundary conditions. Unlike traditional hierarchical clock trees, there is no reference clock present. As a result, the synchronization dynamics in such networks self-organize according to the properties of the nodes and the network. This can lead to so-called *mutually synchronized states*. Such states are characterized by the asymptotic frequencies of the oscillators being equal and the phase differences between nodes being constant in time [16], [55]. Hence, the theoretical ansatz to study the existence of synchronized states is

$$\varphi_k(t) = \Omega_{\text{NET}} t + \varphi_k, \quad (4)$$

where Ω_{NET} is the angular network frequency in the coupling path and the synchronized output frequency of each coupled node. φ_k denotes the initial phase-offset of node k .

Assuming that in a synchronized state all perturbations have decayed and that all nodes in the network are identical, the ansatz in Eq. 4 inserted into the dynamic model in Eq. (1-3)

results in the following set of implicit expressions

$$N \Omega_{\text{NET}} = g \left(G_{\text{LF}} \left(V_{\text{bias}} + \frac{G_{\text{PD}}}{E_k} \times \sum_{i=1}^M d_{ki} \Delta \left[-\Omega_{\text{NET}} \tau_{\text{delay},ki} - \varphi_{\text{mode},ki} \right] \right) \right) \quad (5)$$

G_{LF} denotes the LF steady state gain, including the PD gain G_{PD} , $\Delta(\cdot)$ the normalized triangular phase-error transfer function of an XOR based PD with an amplitude of one, $\tau_{\text{delay},ki}$ the effective time delay and $\varphi_{\text{mode},ki} = \varphi_k - \varphi_i$ the phase difference between node k and i . This constant phase difference is the so-called *mode locking phase difference* and is induced by the periodicity of the PD's phase error transfer function and depends on the network topology [16], [46], [56].

Eq. 5 can be used to find all existing states and their properties $\{\Omega_{\text{NET}}, \varphi_{\text{mode},ki}\}$. Whether or not these are stable has to be determined studying the response of a state to phase perturbations. If a state is asymptotically stable, it can be observed in a system, e.g. during measurements. The set of Eq. 5 reveals that the synchronized state depends not only on the intrinsic parameters of each node, such as the loop bandwidth and loop gain, but also on the network topology and the effective time delay between coupled nodes.

C. Entrainment of Mutually Synchronized States

In order to study whether self-organized synchronized states can be entrained by a reference oscillator, a fixed angular reference frequency ω_{REF} is injected to one node of the network of the mutually coupled PLLs. If the entrainment is successful, all nodes of the network will oscillate with the frequency of the reference, which is formally expressed by

$$\Omega_{\text{NET}} = \omega_{\text{REF}}. \quad (6)$$

Therefore, possible stable states can be predicted inserting Eq. 6 into Eq. 5. Then, the properties of existing entrained synchronized states are obtained by evaluating

$$\frac{g^{-1}(N \omega_{\text{REF}}) - g^{-1}(N \omega_0)}{G_{\text{FF}}} = \frac{1}{E_k} \sum_{i=1}^M d_{ki} \Delta \left[-\omega_{\text{REF}} \tau_{\text{delay},ki} - \varphi_{\text{mode},ki} \right]. \quad (7)$$

$G_{\text{FF}} = G_{\text{PD}} G_{\text{LF}}$ denotes the steady state gain of PD and LF in the feed-forward path and ω_0 is the divided closed loop free-running frequency of each PLL node, assuming that there is no external signal. $g^{-1}(\cdot)$ denotes the inverse of the frequency response function of the VCO. Evaluation for a given frequency yields the corresponding tuning voltage.

1) *Chain Topology*: When entraining a network of mutually coupled nodes in chain topology, illustrated in Fig. 3, the cross-coupling output frequency of node A is forced towards the reference frequency ω_{REF} . Node A affects the frequency of node B, and so on. If the entrainment is successful, the frequencies of all nodes become equal asymptotically. Then, the phase differences can be calculated from Eq. 7 starting with the equation for the last oscillator of the chain – in the case presented here, node C. For the following analysis, it is

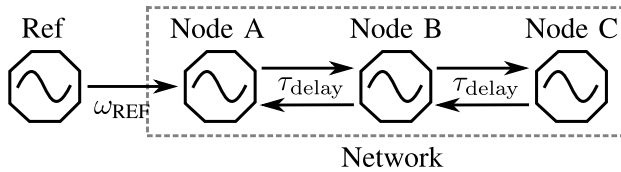


Fig. 3. Representation of a network with three mutually coupled PLL nodes in chain topology. Node A is entrained by an external reference and all cross-coupling delays between the nodes are identical.

assumed that the time delay between all nodes is identical for the bidirectional coupling, so that $\tau_{\text{delay}} = \tau_{\text{delay},ki}$ for any k and i . Thus, for the reverse direction, the phase difference is reversed so that $\varphi_{\text{mode},ki} = -\varphi_{\text{mode},ik}$ applies. The phase differences between the coupled PLL nodes C, B and A are

$$\varphi_{\text{mode,CB}} = -\omega_{\text{REF}} \tau_{\text{delay}} - \Delta^{-1} \left[\frac{g^{-1}(N\omega_{\text{REF}}) - g^{-1}(N\omega_0)}{G_{\text{FF}}} \right], \quad (8)$$

$$\varphi_{\text{mode,BA}} = -\omega_{\text{REF}} \tau_{\text{delay}} - \Delta^{-1} \left[\frac{2(g^{-1}(N\omega_{\text{REF}}) - g^{-1}(N\omega_0))}{G_{\text{FF}}} - \Delta(-\omega_{\text{REF}} \tau_{\text{delay}} + \varphi_{\text{mode,CB}}) \right], \quad (9)$$

and $\varphi_{\text{mode,AR}}$ for the phase difference between node A and the reference node R

$$\varphi_{\text{mode,AR}} = -\omega_{\text{REF}} \tau_{\text{delay}} - \Delta^{-1} \left[\frac{2(g^{-1}(N\omega_{\text{REF}}) - g^{-1}(N\omega_0))}{G_{\text{FF}}} - \Delta(-\omega_{\text{REF}} \tau_{\text{delay}} + \varphi_{\text{mode,BA}}) \right]. \quad (10)$$

To predict the range in which a node of the mutually connected network can follow the reference frequency ω_{REF} , the argument of the inverse phase-error transfer function $\Delta^{-1}(\cdot)$ of the previously obtained phase differences between nodes is evaluated. The set of values of $\Delta(\cdot) \in [-1, 1]$, becomes the domain set of the inverse function. Hence, the argument of $\Delta^{-1}(\cdot)$ in Eq. (8-10) must be in this range. In consequence, the range of ω_{REF} that each node individually can follow in the chain topology can be obtained from evaluating the conditions

$$\begin{aligned} \left| \frac{g^{-1}(N\omega_{\text{REF}}) - g^{-1}(N\omega_0)}{G_{\text{FF}}} \right| &\leq 1, \\ \left| \frac{2(g^{-1}(N\omega_{\text{REF}}) - g^{-1}(N\omega_0))}{G_{\text{FF}}} - A \right| &\leq 1, \\ \left| \frac{2(g^{-1}(N\omega_{\text{REF}}) - g^{-1}(N\omega_0))}{G_{\text{FF}}} - B \right| &\leq 1, \end{aligned} \quad (11)$$

where

$$A = \Delta \left[-2\omega_{\text{REF}} \tau_{\text{delay}} + \Delta^{-1} \left(\frac{g^{-1}(N\omega_{\text{REF}}) - g^{-1}(N\omega_0)}{G_{\text{FF}}} \right) \right], \quad (12)$$

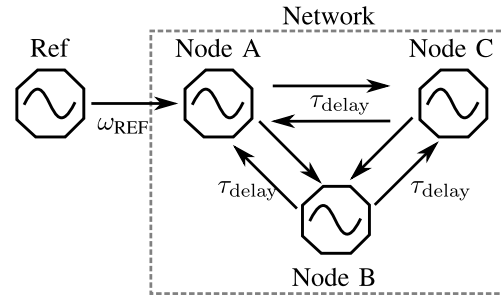


Fig. 4. Representation of a network with three mutually coupled PLL nodes in ring topology. Node A is entrained by an external reference and all cross-coupling delays between the nodes are identical.

$$B = \Delta \left[-2\omega_{\text{REF}} \tau_{\text{delay}} + \Delta^{-1} \left(\frac{g^{-1}(N\omega_{\text{REF}}) - g^{-1}(N\omega_0)}{G_{\text{FF}}} - A \right) \right]. \quad (13)$$

Thus, the range in which the network can follow the reference is given by Eq. 11 for node C, B and A when all conditions are met. Eq. 12 and Eq. 13 represent the delayed interactions between nodes C and B from Eq. 9 and nodes B and A from Eq. 10. This reveals that the difference between the tuning voltage of the reference oscillator and the tuning voltages of the free-running oscillators must be within a certain interval so that the network of coupled oscillators is able to follow the reference.

2) *Ring Topology*: The network of three mutually coupled PLL nodes in ring configuration is shown in Fig. 4. All nodes are connected bidirectionally with the same cross-coupling time delay τ_{delay} between them. The phase differences are calculated from Eq. 7 as in the case of the chain topology and are given by

$$\varphi_{\text{mode,CB}} = -\omega_{\text{REF}} \tau_{\text{delay}} - \Delta^{-1} \left[\frac{2(g^{-1}(N\omega_{\text{REF}}) - g^{-1}(N\omega_0))}{G_{\text{FF}}} - \Delta(-\omega_{\text{REF}} \tau_{\text{delay}} - \varphi_{\text{mode,CB}} - \varphi_{\text{mode,BA}}) \right], \quad (14)$$

$$\varphi_{\text{mode,BA}} = -\omega_{\text{REF}} \tau_{\text{delay}} - \Delta^{-1} \left[\frac{2(g^{-1}(N\omega_{\text{REF}}) - g^{-1}(N\omega_0))}{G_{\text{FF}}} - \Delta(-\omega_{\text{REF}} \tau_{\text{delay}} + \varphi_{\text{mode,CB}}) \right], \quad (15)$$

Due to the relative phase relations, the phase difference between nodes A and C can be determined by

$$\varphi_{\text{mode,AC}} = -\varphi_{\text{mode,BA}} - \varphi_{\text{mode,CB}}. \quad (16)$$

The phase difference $\varphi_{\text{mode,AR}}$ of the node A to the reference node R is given by

$$\varphi_{\text{mode,AR}} = -\omega_{\text{REF}} \tau_{\text{delay}} - \Delta^{-1} \left[\frac{3(g^{-1}(N\omega_{\text{REF}}) - g^{-1}(N\omega_0))}{G_{\text{FF}}} \right]$$

$$\left. \begin{aligned} & -\Delta(-\omega_{\text{REF}}\tau_{\text{delay}} + \varphi_{\text{mode,BA}}) \\ & -\Delta(-\omega_{\text{REF}}\tau_{\text{delay}} - \varphi_{\text{mode,CB}} - \varphi_{\text{mode,BA}}) \end{aligned} \right\}. \quad (17)$$

Similarly as discussed in Section II-C1, Eqs. (14)-(17) are used to obtain the range in which each node of the network can follow the external reference. One finds

$$\left| \frac{2(g^{-1}(N\omega_{\text{REF}}) - g^{-1}(N\omega_0))}{G_{\text{FF}}} - \Delta(-\omega_{\text{REF}}\tau_{\text{delay}} + \varphi_{\text{mode,AC}}) \right| \leq 1, \quad (18)$$

$$\left| \frac{2(g^{-1}(N\omega_{\text{REF}}) - g^{-1}(N\omega_0))}{G_{\text{FF}}} - \Delta(-\omega_{\text{REF}}\tau_{\text{delay}} + \varphi_{\text{mode,BC}}) \right| \leq 1,$$

$$\left| \frac{3(g^{-1}(N\omega_{\text{REF}}) - g^{-1}(N\omega_0))}{G_{\text{FF}}} - \Delta(-\omega_{\text{REF}}\tau_{\text{delay}} + \varphi_{\text{mode,BA}}) - \Delta(-\omega_{\text{REF}}\tau_{\text{delay}} - \varphi_{\text{mode,AR}}) \right| \leq 1,$$

Due to the periodic boundary condition of the ring topology, there is an implicit dependence of the phase difference of each node to its connected nodes. Hence, in contrast to a topology with open boundary conditions, e.g. a chain, the region in which the coupled network follows the reference cannot be determined explicitly.

D. Discussion on Theoretical Findings

In a network of mutually coupled oscillators without entrainment by a reference oscillator, synchronized states self-organized in dependence of the properties of the nodes as well as those of the network. Forcing a self-organized synchronized state with a reference oscillator signal can lead to its entrainment. As a result the notion of a self-organized synchronized state breaks down. One observes, that as the reference frequency deviates from the frequency of the self-organized synchronized state, phase relations different to those of the self-organized synchronized state exist. However, these phase differences result not only from the detuned frequencies or the presence of delays between the reference oscillator and the oscillators as known from the classical hierarchical entrainment [57]. Instead, the phase difference is a result of the delays between the mutually coupled nodes. The detuning between the network and reference frequency is not easy to see, since it is assumed that $\tau_{\text{delay,RA}} = \tau_{\text{delay}}$.

The new architecture can be interpreted as a primary-secondary topology, where the secondary consists of a network of mutually delay-coupled oscillators with internal dynamics. This in turn calls for an in-depth analysis of how the primary or reference frequency affects the properties and stability of the self-organized synchronized state. The non-negligible time delays between the individual nodes of the mutually coupled network must be considered. Furthermore, as shown

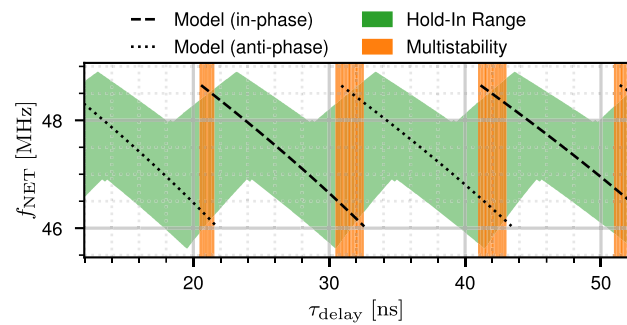


Fig. 5. Numerical solution of stable synchronized coupled network frequencies f_{NET} and hold-in range for an entrained network with three mutually coupled nodes in chain arrangement for time delays τ_{delay} of 12 ns to 52 ns between the nodes. Multistable regions where in-phase and anti-phase stable state exist simultaneously for a given time delay are denoted in orange.

in the previous analysis for the ring and chain topologies, the range in which the network is affected by the reference oscillator is a function of the delays in the mutual coupling and the synchronized states. Note that this is different from the classical case of hierarchical entrainment, where this range depends only on the properties of the PLL.

As an example, this is shown for the network consisting of three nodes in chain topology, see Fig. 5. The asymptotic frequencies of linearly stable in-phase and anti-phase synchronized states for a network without reference are shown with the dashed and dotted line, respectively. With increasing time delay, these states overlap in certain ranges of the time delay. These so-called multistable states are shaded in orange. Which of the two states are observable when a measurement is performed depends on the initial phase configuration and history of the nodes, see [52]. The area highlighted in green, which is wrapped around the synchronized state, is the area in which the mutually coupled network can in principle follow the frequency of the injected reference signal. This area has been obtained by solving Eq. 11. Comparing this range with classical PLL theory, an analogy to the hold-in range can be found. In particular, when considering the first condition in Eq. 11. According to the literature, the hold-in range is defined as the range in which the PLL can follow the reference and track the phase [57]. Note that this is different from the lock-in range, which is the range of stable solutions for which all phase differences and frequencies become stationary. Due to the mutual coupling of the oscillators in the network, there are several conditions for the hold-in range, see Eq. 11 and Eq. 18. These conditions are coupled. All of them have to be fulfilled simultaneously. Consequently, the conditions that lead to the hold range are a function of the synchronized states.

III. PLL NODE DESIGN AND MEASUREMENT SETUP

The validation of the theoretical predictions requires an experimental setup with four identical PLL nodes. Three nodes are used for the network of mutually coupled nodes and one as the reference. The primary requirements for these nodes are flexibility with respect to the network architecture in which they are embedded, as well as mechanisms for calibration. Since the main focus is on systems design, commercially available off-the-shelf components are used to design a modular

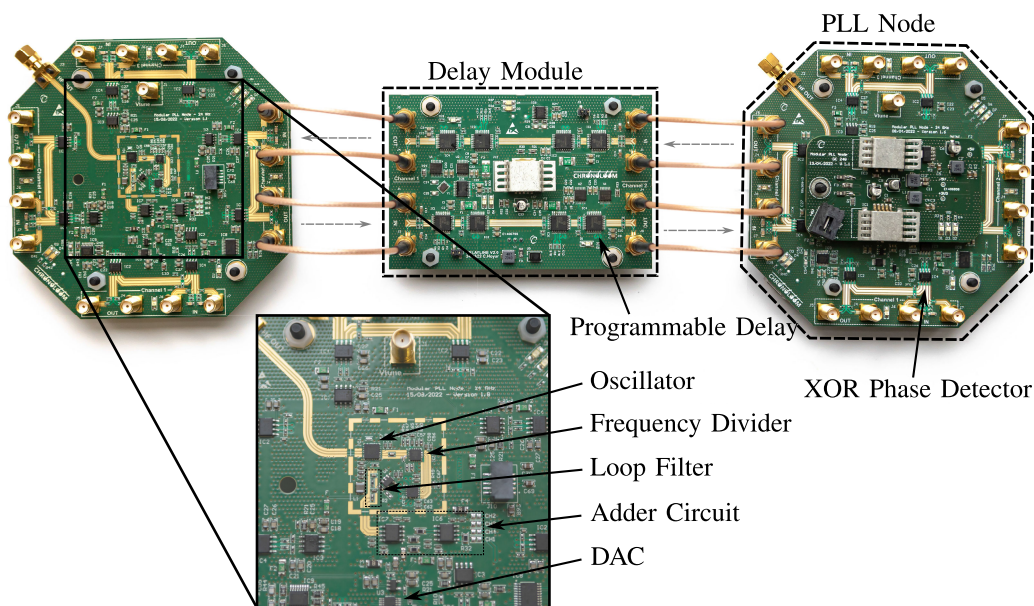


Fig. 6. Minimal working example of two mutually coupled PLL nodes connected via a delay module. The PLL nodes consist of two stacked boards: The lower one is for the PLL and high frequency circuits, the upper one is for the power supply. The cross-coupling connections of the PLL nodes are selected in such a way that they can be connected directly to the delay module or another node without much effort. Due to the modular design, the nodes can also be used in larger scalable networks. The high frequency connection of the VCO output is located at the upper left 45 degree edge. The board size of one PLL node is 120 mm \times 120 mm and the delay module has a size of 113 mm \times 75 mm.

system specifically tailored to the requirements of mutually coupled PLLs. Therefore, considering possible applications in the field of precise localization or tracking [58], [59], [60], an oscillator operating in the 24 GHz band is chosen. To study the coupling behavior with a significant time delay between nodes, the inputs and outputs of the nodes are compatible with differential low-voltage positive emitter coupled logic (LVPECL). This enables the use of cascaded delay chips as a programmable delay between nodes, as shown in Fig. 6. The PLL node and the delay modules provide a USB connection, which allows important system parameters such as the time delay to be set by a computer at runtime.

Each PLL node consists of four input/output channels arranged on all sides of the PCB. Each channel has its own differential output and input interface. Right behind the input of each channel an XOR based phase-detector is placed, which compares the outgoing phase with the incoming one. To simplify the layout, the feedback signal between output and phase detector is inverted. The PD output signal is converted from a differential to a single-ended signal using an operational amplifier before being fed into the adder circuit. The length of all input and output signals are matched, thus the phase of the corresponding signals are equal. Once these signals have been summed up and shifted by the calibration voltage V_{bias} , they are filtered by the LF. Here, a second-order RC low-pass filter with a -3 dB cut-off frequency of 398.1 kHz is used. The high frequency signal of the VCO is divided in frequency by a factor of 512 before it is used as outgoing signal, according to Fig. 1. An additional buffer amplifier enables the measurement of the node's tuning voltage to the oscillator without significantly affecting the closed control loop. The loop bandwidth of the individual PLL node is 497.7 kHz.

The calibration of the closed-loop free-running output frequency of a node is performed using a spectrum analyzer and a digital-to-analog converter (DAC). Based on a python script, the current frequency is measured and the digital value of the DAC is adjusted. Using a high accuracy, low noise voltage reference for the DAC allows very precise calibration of all closed loop free-running oscillator frequencies to 24.3 GHz. The deviation between all nodes is below 5 MHz (0.02%). Moreover, the phase noise of the free-running oscillators is reduced compared to previous work [51], allowing a more accurate synchronization. Note, that the nodes used are not optimized for a specific application, so that some parameters are rather high compared to commercial PLLs.

The realization of the adjustable cross-coupling time-delays between individual PLL nodes is achieved by a delay module with one delay channel for each direction of the coupling between nodes. Each channel consists of four cascaded programmable delay chips, which allow a delay between 11.3 ns and 52.2 ns in total. This delay can be set during the runtime via the USB connection mentioned earlier. Thus, complex automated measurements of the dynamics are possible.

The dynamic properties of the mutual coupled network in chain or ring topology with or without entrainment are studied using the simplified representation of the measurement setup depicted in Fig. 7. The configuration represents the exemplary case of an entrained chain network consisting of three nodes, where the reference signal is injected at node A. The measurement on the cross-coupling frequency level is realized with two oscilloscopes and on high frequency level is measured either with a spectrum analyzer or a real time scope with very high bandwidth.

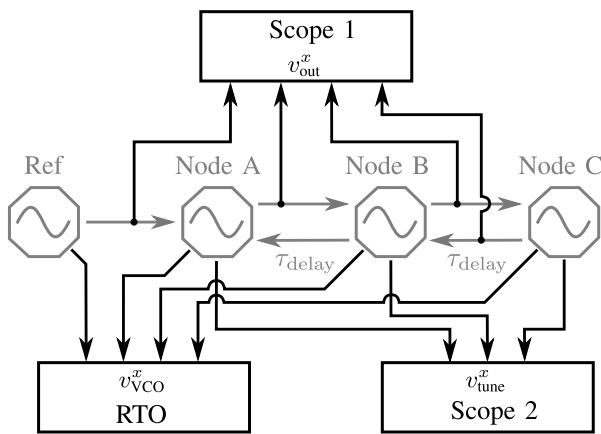


Fig. 7. Sketch of the setup used to measure the chain network topology. Oscilloscope 1 measures the output waveform and extracts its frequency and phase relation, while oscilloscope 2 measures the peak-to-peak tuning voltage and frequency of the individual nodes. The high frequency output signals are measured using a broadband real time oscilloscope (RTO).

To analyze the asymptotic properties of a state, it is necessary to know the frequency of the synchronized state f_{NET} of each node as well as the phase relation $\Delta\varphi_{i,k}$ between the nodes. This is done by capturing the output waveform v_{out}^x of each node with oscilloscope 1 (Rohde & Schwarz RTO 2044) and extracting the necessary data using the oscilloscope's automated measurement function. Each node's dynamical response can be obtained by observing its tuning voltage v_{tune}^x . It reveals insights into the self-organized dynamics for the given measurement conditions, e.g., time delays or entrainment by a reference. For this study the ac component is considered by extracting the peak-to-peak voltage and a possible frequency on the tuning voltage v_{tune}^x with the oscilloscope 2 (Rohde & Schwarz RTO 1044). Another broadband real time oscilloscope (RTO) Keysight UXR 1004A is used to capture the high frequency output signals v_{vco}^x of the oscillator of each PLL node. This recorded time series is later used by the instrument's FFT function to determine the frequency of the individual node. For the calibration routine of each individual node, a Rohde & Schwarz FSU-67 frequency spectrum analyzer is used instead of the broadband RTO. During calibration, the frequency of the node is measured and the voltage V_{bias} is adjusted until the deviation from the desired frequency of 24.3 GHz is less than 500 kHz. Note that the frequency of the node will drift over time due to temperature changes and remaining supply voltage fluctuations.

IV. MEASUREMENT

In the following, the experimental results for the ring and chain topologies studied are presented and analyzed. First, the mutually coupled oscillator networks with self-organized synchronization dynamics are considered in Section IV-A, followed by the cases where networks of mutually coupled nodes are entrained by a reference in the presence of time delays of 35 ns for the chain topology and 36.5 ns for the ring topology in Section IV-B. Particular attention is given to the individual dynamical responses of each node within the mutually coupled network. The analysis of the dynamics

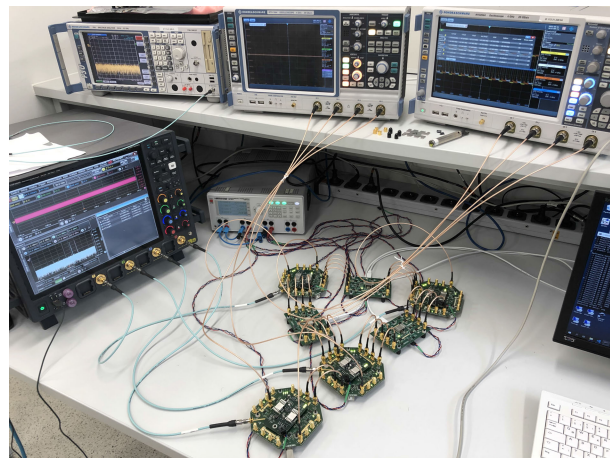
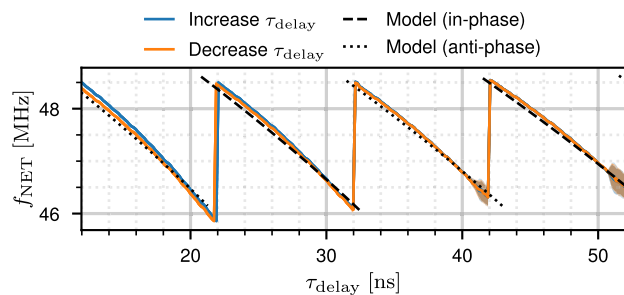
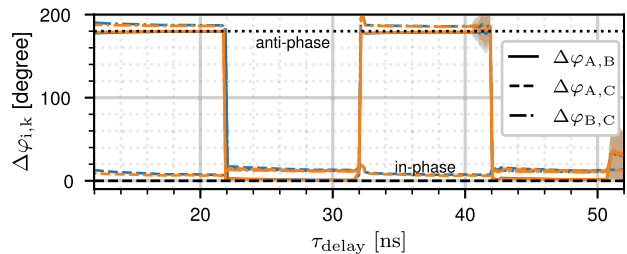


Fig. 8. Photo of the measurement setup in the laboratory where three nodes are mutually coupled in a ring network topology. One of these nodes will be entrained by another PLL node, which serves as a reference. Measurement devices shown starting from top left: spectrum analyzer, oscilloscope 2, oscilloscope 1, and high bandwidth RTO.



(a) Measured network frequency f_{NET} of all nodes and calculated model predictions for synchronized states.



(b) Phase difference $\Delta\varphi_{i,k}$ between nodes.

Fig. 9. Measurements of synchronized states compared to numerical results obtained from Eq. 5 in a network of three mutually coupled nodes in chain topology for increasing and decreasing cross-coupling time delays τ_{delay} . The standard deviations of the network frequency and phase difference are shown in shaded colors.

is carried out for the entire range of time-delay as shown in Section IV-C. The measurement setup used is depicted in Fig. 7 and was adapted to the respective network topology. An example of this is shown in Fig. 8 for a ring topology with entrainment by a reference.

A. Mutual Synchronization

Fig. 9 shows the measured network frequency f_{NET} as well as phase difference $\Delta\varphi_{i,k}$ between nodes for a network of three mutually coupled PLL nodes in a chain topology. The time delay between all nodes is increased linearly from

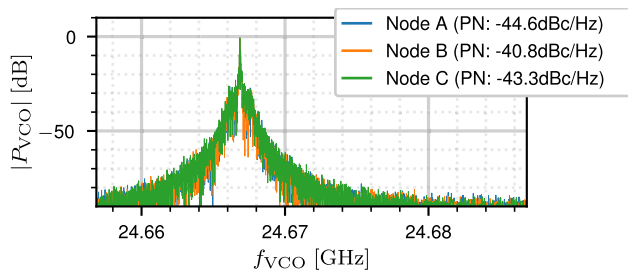


Fig. 10. Measured normalized power spectral densities and phase noise level (PN) at an offset of 1 MHz from the carrier for three mutually coupled PLL nodes in chain topology for a time delay τ_{delay} of 43.97 ns between them. The frequency of the oscillators of all nodes is at 24.666 GHz.

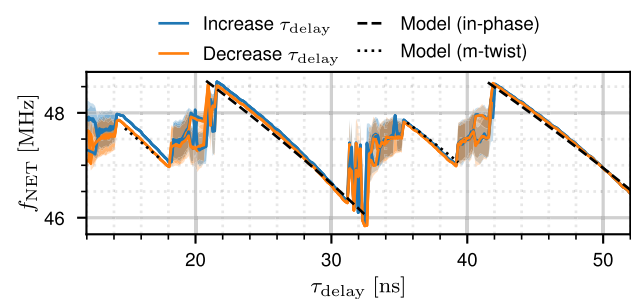
the minimum up to the maximum value of 52.2 ns and then subsequently back to the initial minimum value. All delay modules between the nodes have the same time delay τ_{delay} and the coupling between the nodes is always enabled during the entire sweep.

It can be seen, that a stable synchronized state can be found for almost all time delays. The measured network frequency f_{NET} of all nodes, shown in Fig. 9(a), of synchronized states has a maximum standard deviation of 256 kHz at a delay of 51.7 ns, while the average standard deviation is 18.59 kHz for stable synchronized states. The increase and subsequent decrease of the time delay reveals regimes where multiple synchronized states are stable for a given time delay. This can be seen e.g. at a time delay τ_{delay} of 21.5 ns.

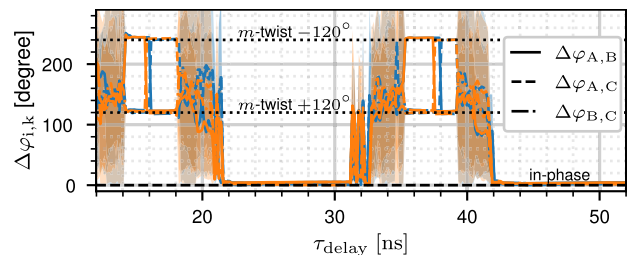
The properties of synchronized states measured in the experimental setups is in good agreement with the theoretical predictions, given by Eq. 5. For such a network topology with open boundary condition, stable states with in- or anti-phase mode-locking phase difference $\varphi_{\text{mode},ki}$ can be observed, as shown in Fig. 9(b). Moreover, it can be seen that the phase difference $\Delta\varphi_{A,C}$ between the two outer nodes A and C always stays in an in-phase relation. For time delays greater than 40 ns instabilities emerge.

Fig. 10 shows the measured frequency spectrum of the high-frequency outputs of all mutually coupled PLL nodes in chain network topology at a time delay of 43.97 ns. The center frequency of all node's high frequency oscillator output is 24.666 GHz and the deviation between them is below the resolution bandwidth of 3.8 kHz of the RTO's FFT function. The phase noise (PN) at a distance of 1 MHz from the center frequency is between -44.64 dBc/Hz and -40.83 dBc/Hz. Due to component availability, a different reference voltage source was used for the DAC of node B in this measurement. The phase noise is averaged over 20 samples, which are in a span of 40 kHz around the offset of 1 MHz on both sidebands. In this way, measurement and extraction artifacts can be reduced. The mean phase noise of the free-running nodes is -44.42 dBc/Hz and -38.25 dBc/Hz for node B, respectively.

The measurements in the network of three mutually coupled PLL nodes in ring topology without entrainment are carried out similarly. Due to the periodic boundary condition of the ring topology, so-called m -twist states can be observed. For these, phase differences between individual nodes arise which correspond to $\Delta\varphi_{i,k} = 2\pi m/M$, where $m \in \{0, \dots, M-1\}$ [56]. The 0-twist corresponds to zero



(a) Measured network frequency f_{NET} of all nodes and calculated model predictions for synchronized states.



(b) Phase difference $\Delta\varphi_{i,k}$ between nodes.

Fig. 11. Measurements of synchronized states compared to numerical results obtained from Eq. 5 in a network of three mutually coupled nodes in ring topology for increasing and decreasing cross-coupling time delays τ_{delay} . The standard deviation in network frequency and phase difference are shown in shaded colors.

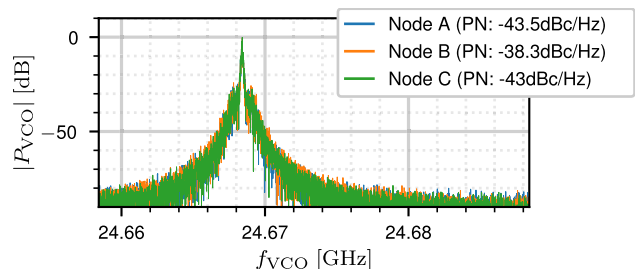


Fig. 12. Measured normalized power spectral densities and phase noise level (PN) at an offset of 1 MHz from the carrier for three mutually coupled PLL nodes in ring topology for a time delay τ_{delay} of 43.97 ns between them. The frequency of the oscillators of all nodes is at 24.668 GHz.

phase differences and hence to an in-phase configuration. In a ring with three mutually coupled nodes, the phase difference $\Delta\varphi_{i,k}$ for the 1-twist are $\pm 120^\circ$ and $\mp 120^\circ$ for the 2-twist.

Fig. 11(a) shows that the predicted frequencies for synchronized 1-twist and 2-twist states are in good agreement with the measurements. The average standard deviation is 19.12 kHz for all stable synchronized states within the time delay range analyzed. For the delay range of approximately 14 ns and 18 ns as well as between 35 ns and 39 ns m -twist state can be observed, as shown in Fig. 11(b). Between the stable synchronous states there are time delays where no stable synchronization was observed.

The measured high-frequency spectrum indicates an identical center frequency of 24.668 GHz for all nodes in the network. The difference between the nodes is also below the resolution bandwidth of 3.8 kHz of the RTO. The phase noise at a distance of 1 MHz from the carrier is between -38.26 dBc/Hz and -43.51 dBc/Hz, as shown in Fig. 12. This is in the same range as for the chain topology.

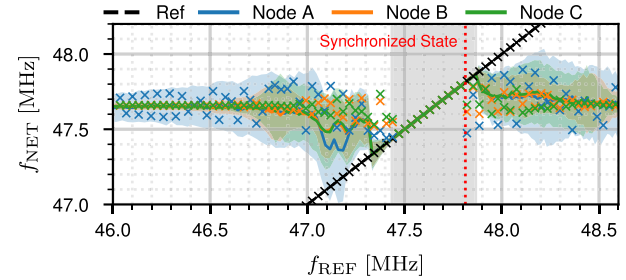
B. Entrainment of Mutual Synchronization for Fixed Delays

This section discusses the effect of unidirectional injection of a reference frequency into the network of mutually coupled nodes. The time delay τ_{delay} between the nodes in the ring or chain topology is constant as the frequency of the reference f_{REF} is varied. An additional PLL node serves as the reference oscillator. Its frequency can be linearly swept using the calibration voltage V_{bias} . The tuning voltage of each node in the network is measured during this parameter sweep. Using an automatic measurement function of the oscilloscope, the frequency f_{tune} and the peak-to-peak voltage $V_{\text{pp,tune}}$ of these experimentally obtained tuning voltages are extracted. From these measures, the lock-in range of the network of mutually coupled PLLs can be identified. Following the definition of the lock-in range it is found where all output frequencies are identical and both measures of the tuning voltages are zero. In the following diagrams this is indicated by the gray region. Note that the tuning voltage within this range still has a constant dc voltage that determines the frequency of the VCO.

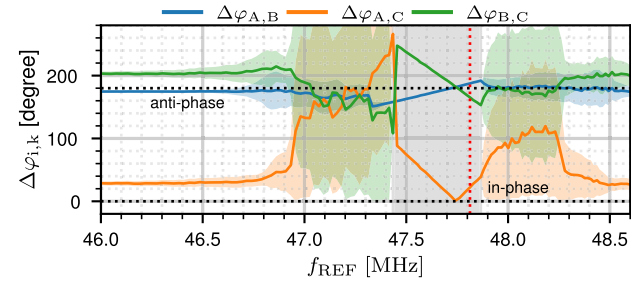
The measurement and numerical results of the chain topology at a time delay τ_{delay} of 35 ns between all nodes are shown in Fig. 13. The numerical results are extracted from time domain simulations of the dynamical model Eqs. (1-3) with an linear VCO response approximation and for ideal filtering of intermodulation products of the PD. The upper diagram, Fig. 13(a), depicts the network frequency f_{NET} of each node as a function of the frequency f_{REF} injected by the reference. The results of the simulations of each node are plotted using markers. The frequencies of the synchronized states obtained from the simulation of the dynamics, given by Eq. 5. The simulated network frequencies are in good agreement with the measured results. The corresponding measured phase relations are given in Fig. 13(b).

Based on these measurements, a range can be extracted in which the frequency of all nodes are identical to the reference frequency. This, so called lock-in range, is between 47.43 MHz and 47.86 MHz denoted by the gray region. All standard deviations of phase relations $\Delta\varphi_{i,k}$ between coupled nodes is below 0.193° within this range. The standard deviation of the network frequencies of node A is 18.4 kHz, of node B is 20.4 kHz, and of node C is 17.0 kHz. Furthermore, it is observed that the phase differences are close to the predicted mutually synchronized state for a non-entrained network with a frequency of 47.81 MHz. At this point, the phase difference between nodes A to B and B to C are in anti-phase, and between nodes A to C it is in an in-phase relation during entrainment. Hence, inside the hold-in range the frequencies of the nodes in the network of mutually coupled nodes are at least partially pulled towards the reference frequency. Within this range there is the lock-in range where the entrainment is successful and all nodes have the same frequency as the reference node.

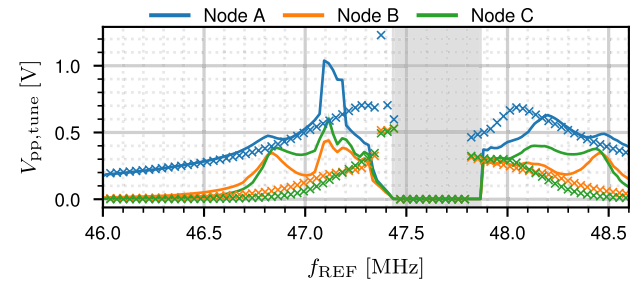
The measured peak-to-peak voltage $V_{\text{pp,tune}}$ of the tuning voltage in Fig. 13(c) and its frequency in Fig. 13(d) confirms this extracted lock-in range. Both, the frequency f_{tune} and the peak-to-peak voltage $V_{\text{pp,tune}}$ are close to zero within this range. The values of both quantities extracted from simulations are also in good agreement with these measurements. The



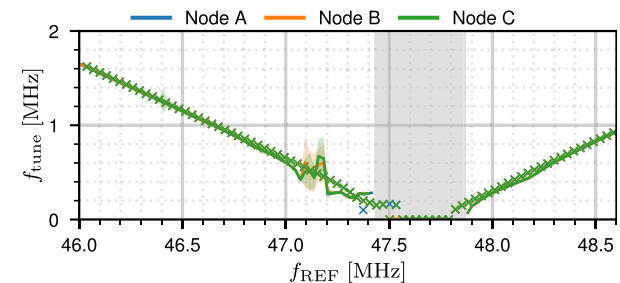
(a) Measured (line) and results of time domain simulation (marker) mean network frequency f_{NET} versus time reference frequency f_{REF} . The red line indicates the predicted mutually synchronized state for the case of no entrainment.



(b) Measured phase differences $\Delta\varphi_{i,k}$ between coupled nodes versus reference frequency f_{REF} . The red line indicates the predicted mutually synchronized state for the case of no entrainment.



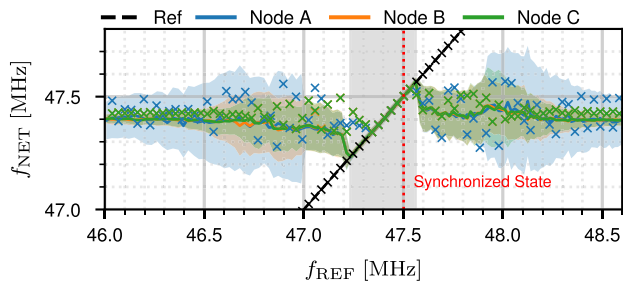
(c) Measured (line) and simulated (marker) peak-to-peak tuning voltage $V_{\text{pp,tune}}$ of each node versus reference frequency f_{REF} .



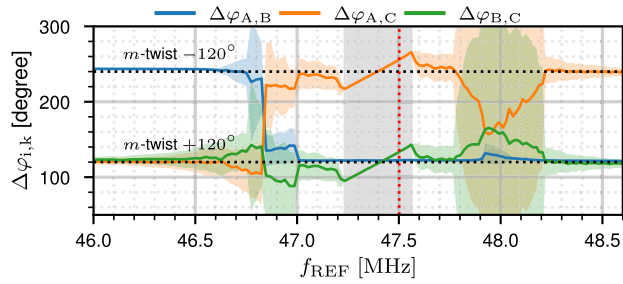
(d) Measured (line) and simulated (marker) tuning voltage frequency f_{tune} of each node versus reference frequency f_{REF} .

Fig. 13. Entrainment of a network with three mutually coupled nodes in chain topology at a time delay τ_{delay} of 35 ns. The gray region denotes the lock-in range extracted from the measurements. The standard deviation of each measured trace is shown in shaded colors.

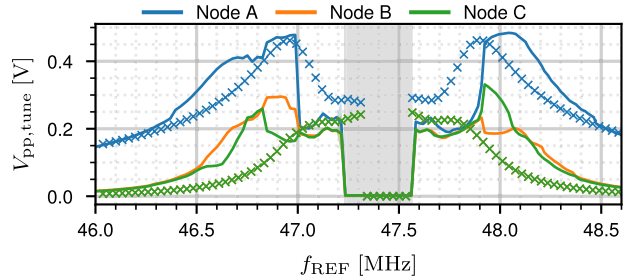
hold-in range in which the network is affected by the reference frequency f_{REF} is between 46.5 MHz and 49.1 MHz. Within this hold-in range, dynamic interactions between the coupled nodes are evident. Furthermore, a strong effect on the entrained node A can be observed. Its control voltage oscillations set in for reference frequencies outside the hold-in range and have



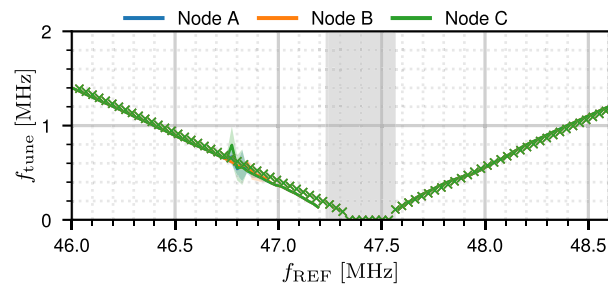
(a) Measured (line) and results of time domain simulation (marker) mean network frequency f_{NET} versus reference frequency f_{REF} . The red line indicates the predicted mutually synchronized state for the case of no entrainment.



(b) Measured phase differences $\Delta\varphi_{i,k}$ between coupled nodes versus reference frequency f_{REF} . The red line indicates the predicted mutually synchronized state for the case of no entrainment.



(c) Measured (line) and simulated (marker) peak-to-peak tuning voltage $V_{\text{pp,tune}}$ of each node versus reference frequency f_{REF} .

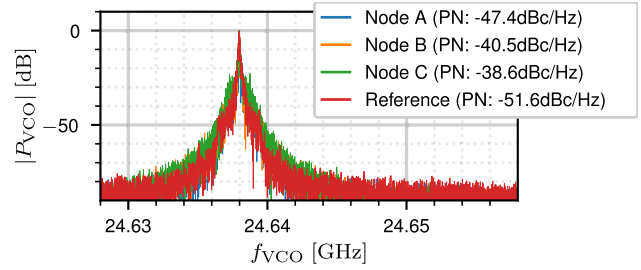


(d) Measured (line) and simulated (marker) tuning voltage frequency f_{tune} of each node versus reference frequency f_{REF} .

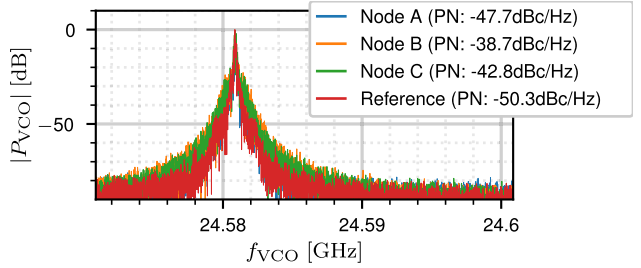
Fig. 14. Entrainment of a network with three mutually coupled nodes in ring topology at a time delay τ_{delay} of 36.5 ns. The gray region denotes the lock-range extracted from the measurements. The standard deviation of each measured trace is shown in shaded colors.

a much larger peak-to-peak voltage $V_{\text{pp,tune}}$ compared to node B and C. This is most probably due to the forcing of node by the reference node.

Fig. 14 shows the measurement results of the ring topology. Qualitatively similar dynamics compared to the chain topology can be observed for the frequency of the coupled nodes.



(a) Measured PSD for a chain topology with three coupled nodes during entrainment. The frequency of all nodes can be found at 24.638 GHz.



(b) Measured PSD for a ring topology with three coupled nodes during entrainment. The frequency of all nodes can be found at 24.581 GHz.

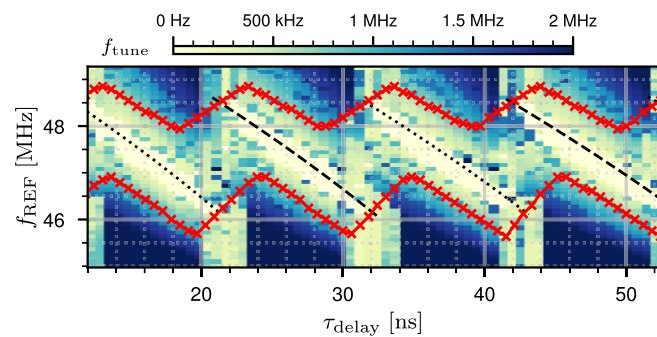
Fig. 15. Measured normalized power spectral densities (PSDs) and phase noise level (PN) at an offset of 1 MHz from the carrier for the entrainment of a network with three mutually coupled PLL Nodes in chain or ring topology for time delay τ_{delay} of 43.97 ns between nodes.

The lock-in range extracted from the measurement is between 47.23 MHz and 47.56 MHz, as denoted by the gray region in Fig. 14(a). Within this range, the standard deviation of the network frequencies of all coupled nodes is found to be below 20.2 kHz and the standard deviation of the phase differences is below 0.199° . These measured deviations are determined during a time interval of 4 s at given frequency f_{REF} . The point at which the phases of the nodes are in a $\pm 120^\circ$ m -twist phase relation is close to the synchronized state in the case without entrainment at 47.5 MHz, as shown in Fig. 14(b).

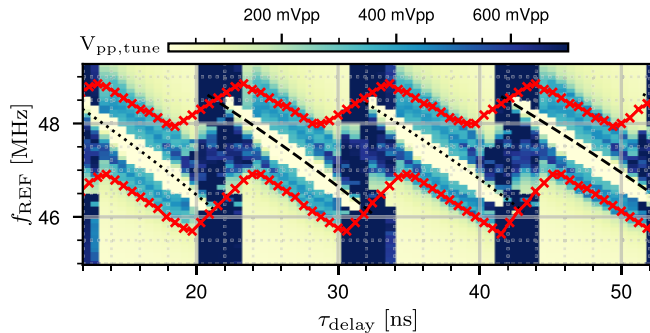
The measured frequency f_{tune} and peak-to-peak amplitude $V_{\text{pp,tune}}$ of the tuning voltage modulation confirms the lock-in range, shown in Fig. 14(c) and Fig. 14(d). Compared to node B and C, the peak-to-peak voltage on the tuning signal of node A is significantly higher. The frequency f_{tune} of the oscillation is identical for all nodes outside the lock-in range and increases linearly with the distance to the lock-in range in the studied frequency range of f_{REF} . The simulated $V_{\text{pp,tune}}$ of nodes B and C is identical for the given f_{REF} . The measurements confirm the simulation results qualitatively and quantitatively. The maximum difference between $V_{\text{pp,tune}}$ of nodes B and C is about 143 mV.

The measured normalized power spectral densities for the ring and chain topology at a time delay τ_{delay} of 43.97 ns between all nodes in the network are depicted in Fig. 15. The center frequency of the high frequency oscillator output of all nodes is 24.638 GHz for the chain and 24.581 GHz for the ring arrangement. In both cases, the deviation between them is below the resolution bandwidth of 3.8 kHz. The phase noise was also averaged in a span of 40 kHz around the offset of 1 MHz on both sidebands.

The measured phase noise at a frequency offset of 1 MHz to the carrier is for the reference between -51.57 dBc/Hz



(a) Mean frequency f_{tune} of the tuning voltage of all nodes during entrainment.



(b) Mean peak-to-peak voltage $V_{\text{pp,tune}}$ of the tuning voltage of all nodes during entrainment.

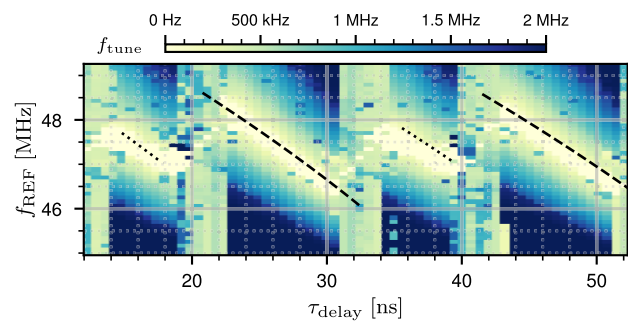
Fig. 16. Measured entrainment of a network with three mutually coupled PLL nodes in chain topology versus cross-coupling time delays τ_{delay} . The black lines indicate the simulated synchronized states in the case of a network without an injected reference. The dotted line corresponds to the anti-phase and the dashed line to the in-phase synchronized state. The red lines bound the determined range in which the network can follow the reference.

and -50.26 dBc/Hz. The entrained node A has a phase noise of -47.7 dBc/Hz respectively -47.37 dBc/Hz in both network topologies studied. The other two nodes have a phase noise of between -38.59 dBc/Hz and -40.51 dBc/Hz in chain arrangement, as shown in Fig. 15(a) and between -38.71 dBc/Hz and -42.84 dBc/Hz in ring topology, depicted in Fig. 15(b).

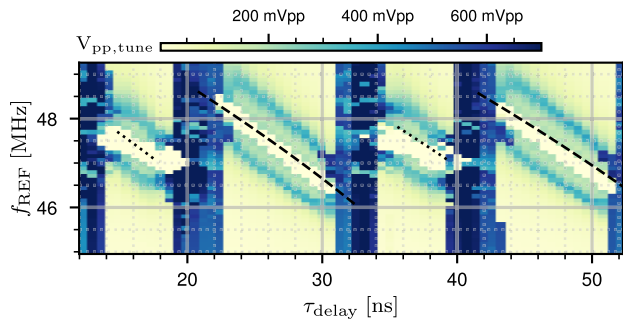
C. Parameter Space Plots of Hold- and Lock-In Range

In the next step, the analysis introduced in the last subsection is carried out for time delays ranging from 11.3 ns to 52.3 ns. The resulting parameter space plots show the average value over all nodes of the frequency f_{tune} and peak-to-peak voltage $V_{\text{pp,tune}}$ of the tuning voltage for each delay τ_{delay} and reference frequency f_{REF} value in a heat map. Therefore, both indicators of this ensemble average are color coded. The lighter color indicates a low value and the darker color a high value, see the color bars on top of each figure. When both measured quantities are close to zero, no dynamic change of the tuning voltage is detected, which means that the PLL nodes are phase-locked to the injected reference.

Fig. 16 shows the dynamical properties of an entrained mutual coupled network with three PLL nodes in chain topology. From the mean frequency f_{tune} of the tuning voltage in Fig. 16(a) it can be seen that the frequency decreases when f_{REF} is close to a synchronized state. No conclusive value of



(a) Mean frequency f_{tune} of the tuning voltage of all nodes during entrainment.



(b) Mean peak-to-peak voltage $V_{\text{pp,tune}}$ of the tuning voltage of all nodes during entrainment.

Fig. 17. Measured entrainment of a network with three mutually coupled PLL nodes in ring topology versus cross-coupling time delays τ_{delay} . The black lines indicate the simulated synchronized states in the case of a network without an injected reference. The dotted line corresponds to the anti-phase and the dashed line to the in-phase synchronized state. The red lines bound the determined range in which the network can follow the reference.

f_{tune} can be detected in the ranges of the time delay where multistability occurs, such as between 20 ns and 23.5 ns.

It can be observed that within the hold-in range the peak-to-peak voltage $V_{\text{pp,tune}}$, shown in Fig. 16(b), shows two qualitatively different behaviors. Close to the frequency of the self-organized synchronized states shown by the dashed and dotted lines, $V_{\text{pp,tune}}$ tends towards zero, i.e., oscillations of the tuning voltage are suppressed. This is the lock-in range where the entire network locks to the reference. Outside this lock-in range the tuning voltage oscillates and thereby affects the high frequency output of the PLLs, see e.g., Fig. 13(d). In regimes where multistability can occur the lock-in ranges are decreased. Furthermore, no clear trends in the dynamics of the tuning voltages are visible.

A qualitatively similar behavior can also be observed for the network in ring topology, which is presented in Fig. 17. In close proximity to the frequency of the self-organized synchronized state, the network can lock to the frequency of the reference. This is evident from the low $V_{\text{pp,tune}}$ and f_{tune} values and corresponds to the lock-in range. As the deviation between the reference frequency and that of the synchronized state increases, the frequency of the tuning voltage increases almost linearly, as shown in Fig. 17(a). The peak-to-peak voltage, however, increases and then decreases again subsequently.

Given the hold-in ranges shown for the entrainment of the chain topology in Fig. 16(b) suggest that the boundaries of

the hold-in range are defined by the dynamics of the tuning voltage. Hence, in Fig. 17(b) the hold-in range is found where the peak-to-peak voltage is zero (lock-in range), and within the regimes where $V_{pp,tune}$ is far from zero, see shoulders in the parameter space plots. These represent where the tuning voltage oscillates with large amplitude. Note that there is a qualitatively different behavior around the m -twist state with $m > 0$. The lock-in ranges associated to these twist states can be seen to extend beyond regimes of time delays where twist solutions for self-organized states exists, see e.g. Fig. 11(a) and Fig. 17(a) at a delay of 19 ns.

V. CONCLUSION AND DISCUSSION

The research presented here studies whether hierarchical and non-hierarchical synchronization concepts can be combined to achieve a robust synchronization layer in the presence of considerable cross-coupling time delays. In general, in hierarchical synchronization approaches, cross-coupling time delays translate into phase-differences between individual oscillators. This is not the case in non-hierarchical synchronization concepts wherein oscillators in a network are mutually coupled without a reference. As a result the dynamics self-organize and can lead to synchronized states with a common global network frequency and hence constant phase relations. Given these qualitative difference between the two approaches, this work asks how the entrainment affects a network of mutually delay-coupled oscillators.

Using well known concepts from classical PLL theory, combined with a theoretical framework for studying mutually coupled oscillators, a hold-in range can be obtained analytically. It represents the regime in which the self-organized dynamics of the mutually coupled oscillators are affected by the external reference. This leads to the question whether the self-organized synchronous state can be abstracted as a secondary oscillator. This is not supported by the observations made from the measurements. These reveal, that the hold-in range is a function of the cross-coupling time delays within the entrained network. Furthermore, the self-organization dynamics depend also on the network topology as well as the characteristics of each individual node. These factors combined lead to complex internal dynamics in the network of mutually coupled oscillators. Consequently, a generic abstraction of the network as a secondary oscillator in a hierarchical synchronization approach cannot be supported.

Measurements of the entrainment of mutual synchronization were carried out for a network in a chain and in a ring topology with three mutually coupled nodes. These show, how the frequencies of self-organized synchronous states depend on the cross-coupling time delays. Similarly, the hold-in range becomes a function of these delays. It is bounded by a maximum detuning between the frequency of the reference and that of the self-organized states. As a result, entrainment can only be achieved within the hold-in range. More specifically, stable entrainment of synchronized states with a constant global frequency is only achieved within the lock-in range, which lies entirely within the hold-in range. Hence, the lock-in range specifies the range in which the frequency of the self-organized

synchronous state can be pulled sufficiently to match that of the reference. At the same time, phase difference between the nodes of the network arise if there is a detuning between the frequency of the reference and that of the state. The measurements are in good agreement with the analytical and numerical predictions of the theory presented in this work. Hence, this work shows that the synchronization dynamics of a network of mutually delay-coupled oscillators can successfully be entrained by an external reference oscillator. Note that this can also be observed for values of the cross-coupling time delay where no self-organized state exists or is stable.

REFERENCES

- [1] M. B. Brilliant, "The determination of frequency in systems of mutually synchronized oscillators," *Bell Syst. Tech. J.*, vol. 45, no. 10, pp. 1737–1748, Dec. 1966.
- [2] A. Gersho and B. J. Karafin, "Mutual synchronization of geographically separated oscillators," *Bell Syst. Tech. J.*, vol. 45, no. 10, pp. 1689–1704, Dec. 1966.
- [3] M. Karnaugh, "A model for the organic synchronization of communications systems," *Bell Syst. Tech. J.*, vol. 45, no. 10, pp. 1705–1735, Dec. 1966.
- [4] M. R. Miller, "Feasibility studies of synchronised-oscillator systems for p.c.m. telephone networks," *Proc. Inst. Electr. Eng.*, vol. 116, no. 7, p. 1135, 1969.
- [5] A. Weinberg and B. Liu, "Noise and transmission delays in mutual synchronization systems," *IEEE Trans. Aerosp. Electron. Syst.*, vol. AES-11, no. 5, pp. 756–767, Sep. 1975.
- [6] J. C. Candy and M. Karnaugh, "Organic synchronization: Design of the controls and some simulation results," *Bell System Tech. J.*, vol. 47, no. 2, pp. 227–259, Feb. 1968.
- [7] J. R. Pierce, "Synchronizing digital networks," *Bell System Tech. J.*, vol. 48, no. 3, pp. 615–636, Mar. 1969.
- [8] M. Williard, "Analysis of a system of mutually synchronized oscillators," *IEEE Trans. Commun.*, vol. COM-18, no. 5, pp. 467–483, Oct. 1970.
- [9] H. Stover, "Network timing/synchronization for defense communications," *IEEE Trans. Commun.*, vol. COM-28, no. 8, pp. 1234–1244, Aug. 1980.
- [10] P. Kartaschoff, P. Andre Probst, and P. Vörös, "A network timing concept for Switzerland," in *Proc. 17th Annu. Precise Time Interval Syst. Appl. Meeting*, Dec. 1985, pp. 287–302. [Online]. Available: <https://www.ion.org/publications/abstract.cfm?articleID=16143>
- [11] H. Hartmann and E. Steiner, "Synchronization techniques for digital networks," *IEEE J. Sel. Areas Commun.*, vol. SAC-4, no. 4, pp. 506–513, Jul. 1986.
- [12] D. Mitra, "Network synchronization: Analysis of a hybrid of master-slave and mutual synchronization," *IEEE Trans. Commun.*, vol. COM-28, no. 8, pp. 1245–1259, Aug. 1980.
- [13] H. A. Stover, "Overview of timing/synchronization for digital communications," in *Proc. 10th Annu. Precise Time Interval Syst. Appl. Meeting*, Aug. 1978, pp. 1–11. [Online]. Available: <https://ntrs.nasa.gov/citations/19790016575>
- [14] W. Lindsey, F. Ghazvinian, W. C. Hagmann, and K. Dessouky, "Network synchronization," *Proc. IEEE*, vol. 73, no. 10, pp. 1445–1467, Oct. 1985.
- [15] R. L. Mitchell, "Survey of timing/synchronization of operating wideband digital communications networks," in *Proc. 10th Annu. Precise Time Interval (PTI) Appl. Planning Meeting*, Aug. 1978, pp. 405–435. [Online]. Available: <https://ntrs.nasa.gov/citations/19790016576>
- [16] L. Wetzel et al., "Network synchronization revisited: Time delays in mutually coupled oscillators," *IEEE Access*, vol. 10, pp. 80027–80045, 2022.
- [17] M. Spellman, J. Bibb, C. David, and B. Bradley, "Frequency control and digital network synchronization," in *Proc. 31st Annu. Symp. Freq. Control*, Dec. 1977, pp. 436–447.
- [18] A. Sobeih, M. Hack, Z. Liu, and L. Zhang, "Almost peer-to-peer clock synchronization," in *Proc. IEEE Int. Parallel Distrib. Process. Symp.*, Jun. 2007, pp. 1–10.
- [19] S. Bühr, M. Kreissig, and F. Ellinger, "Low power 16 phase ring oscillator and PLL for use in sub-ns time synchronization over Ethernet," in *Proc. 25th IEEE Int. Conf. Electron., Circuits Syst. (ICECS)*, Dec. 2018, pp. 53–56.

- [20] J. E. Abate et al., "AT&T's new approach to the synchronization of telecommunication networks," *IEEE Commun. Mag.*, vol. 27, no. 4, pp. 35–45, Apr. 1989.
- [21] S. Bregni, "A historical perspective on telecommunications network synchronization," *IEEE Commun. Mag.*, vol. 36, no. 6, pp. 158–166, Jun. 1998.
- [22] R. F. Riaz et al., "Stability and transient dynamics of PLLs in theory and experiments," in *Proc. Eur. Conf. Circuit Theory Design (ECCTD)*, Sep. 2020, pp. 1–4.
- [23] J. Lopez-Jimenez, J. L. Gutierrez-Rivas, E. Marin-Lopez, M. Rodriguez-Alvarez, and J. Diaz, "Time as a service based on White Rabbit for finance applications," *IEEE Commun. Mag.*, vol. 58, no. 4, pp. 60–66, Apr. 2020.
- [24] P. V. Estrela and L. Bonebakker, "Challenges deploying PTPv2 in a global financial company," in *Proc. IEEE Int. Symp. Precis. Clock Synchronization Meas., Control Commun. Proc.*, Sep. 2012, pp. 1–6.
- [25] K. Ochs, B. Al Beattie, and S. Jenderny, "An Ising machine solving max-cut problems based on the circuit synthesis of the phase dynamics of a modified Kuramoto model," in *Proc. IEEE Int. Midwest Symp. Circuits Syst. (MWSCAS)*, Aug. 2021, pp. 982–985.
- [26] Y. Li et al., "Sundial: Fault-tolerant clock synchronization for data-centers," in *Proc. 14th USENIX Symp. Operating Syst. Design Implementation. (OSDI)*, Nov. 2020, pp. 1–17. [Online]. Available: <https://www.usenix.org/conference/osdi20/presentation/li-yuliang>
- [27] D. L. Mills, "Internet time synchronization: The network time protocol," *IEEE Trans. Commun.*, vol. 39, no. 10, pp. 1482–1493, Oct. 1991.
- [28] H. Yahata, "Hybrid clock synchronization: Condition for the existence of steady state in a ring network," *Electron. Commun. Jpn. I, Commun.*, vol. 79, no. 8, pp. 24–39, 1996.
- [29] H. Yahata, "Hybrid clock synchronization: The pull-in range of a ring network," *Electron. Commun. Jpn. I, Commun.*, vol. 82, no. 6, pp. 45–59, Jun. 1999.
- [30] E. Zianbetov et al., "Distributed clock generator for synchronous SoC using ADPLL network," in *Proc. IEEE Custom Integr. Circuits Conf.*, Sep. 2013, pp. 1–4.
- [31] P. Teehan, M. Greenstreet, and G. Lemieux, "A survey and taxonomy of GALS design styles," *IEEE Design Test Comput.*, vol. 24, no. 5, pp. 418–428, Sep. 2007.
- [32] E. Koskin, D. Galayko, and E. Blokhina, "A concept of synchronous ADPLL networks in application to small-scale antenna arrays," *IEEE Access*, vol. 6, pp. 18723–18730, 2018.
- [33] E. Koskin, P. Bisiaux, D. Galayko, and E. Blokhina, "All digital phase-locked loop networks for clock generation and distribution: Network stability, convergence and performance," *IEEE Trans. Circuits Syst. I, Reg. Papers*, vol. 68, no. 1, pp. 406–415, Jan. 2021.
- [34] I. W. Sandberg, "On conditions under which it is possible to synchronize digital transmission systems," *Bell System Tech. J.*, vol. 48, no. 6, pp. 1999–2022, Jul. 1969.
- [35] I. W. Sandberg, "Some properties of a nonlinear model of a system for synchronizing digital transmission networks," *Bell System Tech. J.*, vol. 48, no. 9, pp. 2975–2997, Nov. 1969.
- [36] J. Yamato, M. Ono, and S. Usuda, "Synchronization of a PCM integrated telephone network," *IEEE Trans. Commun.*, vol. COM-16, no. 1, pp. 1–11, Feb. 1968.
- [37] A. Katak and W. Lindsey, "A note on the statistical dynamics of two mutually phase-locked oscillators," *IEEE Trans. Commun.*, vol. COM-30, no. 10, pp. 2341–2343, Oct. 1982.
- [38] K. Dessouky and W. Lindsey, "Phase and frequency transfer between mutually synchronized oscillators," *IEEE Trans. Commun.*, vol. COM-32, no. 2, pp. 110–117, Feb. 1984.
- [39] H. J. Choi and W. C. Lindsey, "Phase and frequency transfer analysis of N mutually synchronized oscillators," *IEEE Trans. Aerosp. Electron. Syst.*, vol. AES-20, no. 6, pp. 748–753, Nov. 1984.
- [40] T. Endo and L. O. Chua, "Chaos from two-coupled phase-locked loops," *IEEE Trans. Circuits Syst.*, vol. 37, no. 9, pp. 1183–1187, Sep. 1990.
- [41] H. Tanaka, S. Oishi, and K. Horiuchi, "Synchronization limit and chaos onset in mutually coupled phase-locked loops," in *Proc. APCCAS Asia Pacific Conf. Circuits Syst.*, Dec. 1994, pp. 317–321.
- [42] H. A. Tanaka, S. Oishi, and K. Horiuchi, "Geometric structure of mutually coupled phase-locked loops," *IEEE Trans. Circuits Syst. I, Fundam. Theory Appl.*, vol. 43, no. 6, pp. 438–443, Jun. 1996.
- [43] H.-C. Chang, X. Cao, U. K. Mishra, and R. A. York, "Phase noise in coupled oscillators: Theory and experiment," *IEEE Trans. Microw. Theory Techn.*, vol. 45, no. 5, pp. 604–615, May 1997.
- [44] H.-C. Chang, E. S. Shapiro, and R. A. York, "Influence of the oscillator equivalent circuit on the stable modes of parallel-coupled oscillators," *IEEE Trans. Microw. Theory Techn.*, vol. 45, no. 8, pp. 1232–1239, Aug. 1997.
- [45] B. Ottino-Löffler and S. H. Strogatz, "Comparing the locking threshold for rings and chains of oscillators," *Phys. Rev. E, Stat. Phys. Plasmas Fluids Relat. Interdiscip. Top.*, vol. 94, no. 6, Dec. 2016, Art. no. 062203.
- [46] S. Eydam and M. Wolfrum, "Mode locking in systems of globally coupled phase oscillators," *Phys. Rev. E, Stat. Phys. Plasmas Fluids Relat. Interdiscip. Top.*, vol. 96, no. 5, Nov. 2017, Art. no. 052205.
- [47] P. S. Skardal, "Stability diagram, hysteresis, and critical time delay and frequency for the Kuramoto model with heterogeneous interaction delays," *Int. J. Bifurcation Chaos*, vol. 28, no. 5, May 2018, Art. no. 1830014.
- [48] Y. Liu and Y. Guo, "Synchronization in a Kuramoto model with delay-dependent couplings," *AIP Adv.*, vol. 9, no. 2, Feb. 2019, Art. no. 025026.
- [49] D. Prousalis and L. Wetzel, "Synchronization in the presence of time delays and inertia: Stability criteria," *Phys. Rev. E, Stat. Phys. Plasmas Fluids Relat. Interdiscip. Top.*, vol. 105, no. 1, Jan. 2022, Art. no. 014210.
- [50] A. Pollakis, L. Wetzel, D. J. Jötrg, W. Rave, G. Fettweis, and F. Jütlicher, "Synchronization in networks of mutually delay-coupled phase-locked loops," in *Proc. IEEE Int. Conf. Commun. (ICC)*, vol. 16, no. 11, Nov. 2014, Art. no. 113009.
- [51] C. Hoyer, L. Wetzel, D. Prousalis, J. Wagner, F. Jütlicher, and F. Ellinger, "Mutual synchronization of spatially distributed 24 GHz oscillators up to distances of 500 m," *IEEE Trans. Circuits Syst. II, Exp. Briefs*, vol. 69, no. 9, pp. 3689–3693, Sep. 2022.
- [52] C. Hoyer, L. Wetzel, D. Prousalis, J. Wagner, F. Jütlicher, and F. Ellinger, "Stability analysis of mutually synchronized spatially distributed 24 GHz oscillators," in *Proc. IEEE Int. Instrum. Meas. Technol. Conf. (I2MTC)*, May 2022, pp. 1–6.
- [53] Analog Devices, "HMC739LP4/739LP4E," Analog Devices, Hittie, Wilmington, MA, USA, Version v03.0309, 2020. [Online]. Available: analog.com/media/en/technical-documentation/data-sheets/hmc739.pdf
- [54] C. Hoyer et al., "Mutual synchronization with 24 GHz oscillators," in *Proc. IEEE Int. Symp. Circuits Syst. (ISCAS)*, May 2021, pp. 1–5.
- [55] F. M. Orsatti, R. Carareto, and J. R. C. Piqueira, "Multiple synchronous states in static delay-free mutually connected PLL networks," *Signal Process.*, vol. 90, no. 6, pp. 2072–2082, Jun. 2010.
- [56] G. A. Pratt and J. Nguyen, "Distributed synchronous clocking," *IEEE Trans. Parallel Distrib. Syst.*, vol. 6, no. 3, pp. 314–328, Mar. 1995.
- [57] R. E. Best, *Phase Locked Loops 6/E*. New York, NY, USA: McGraw-Hill, 2007.
- [58] C. Will, P. Vaishnav, A. Chakraborty, and A. Santra, "Human target detection, tracking, and classification using 24-GHz FMCW radar," *IEEE Sensors J.*, vol. 19, no. 17, pp. 7283–7299, Sep. 2019.
- [59] P. Wang et al., "A gesture air-writing tracking method that uses 24 GHz SMO radar SoC," *IEEE Access*, vol. 8, pp. 152728–152741, 2020.
- [60] M. Gottinger et al., "Coherent automotive radar networks: The next generation of radar-based imaging and mapping," *IEEE J. Microw.*, vol. 1, no. 1, pp. 149–163, Jan. 2021.



Christian Hoyer was born in 1992. He received the B.Sc. degree in electrical engineering from the University of Kassel in 2017 and the M.Sc. degree in electrical engineering with focus on high-frequency electronics from the Karlsruhe Institute of Technology (KIT) in 2019. He is currently pursuing the Ph.D. degree in high-frequency analog integrated circuits with the Chair for Circuit Design and Network Theory, Technische Universität Dresden, Germany. His master thesis was done at the Fraunhofer Institute for Applied Solid State Physics IAF, Freiburg, in the field of broadband GaN high-power amplifiers. During his studies, he worked for several research and development projects in industry and research institutes. His main research interests include high-precision synchronization, high-frequency integrated circuits, and oscillators.



Lucas Wetzel received the joint Diploma degrees in physics from Leipzig University and ETH Zürich in 2008 and the Ph.D. degree in physics from the Max Planck Institute for the Physics of Complex Systems, TU Dresden (TUD), in 2012. During his diploma studies, he specialized on micro- and nanosystems, stochastic processes, and nonlinear dynamics. His diploma thesis on the statistical properties of stochastic delay differential equations with additive and multiplicative noise was supervised by Prof. Ulrich Behn. Since 2008, he has been with the

Max Planck Institute for the Physics of Complex Systems. In the following, he arranged a collaboration with the Vodafone Chair Mobile Communications Systems, TUD, and within the Center for Advancing Electronics Dresden, studying mutual synchronization inspired from biological systems and its application to electronic systems. In 2019, he received together with the Chair for Circuit Design and Network Theory, TUD, and the Fraunhofer Institute for Reliability and Microintegration IZM, Dresden, a VIP+ grant from the German Federal Ministry of Education and Research to validate mutual network synchronization. His research interests include nonlinear dynamics in systems with time-delayed interactions and control theoretical approaches to nonlinear systems with the goal to advance ideas from basic research to application. He is a member of the German Physical Society (DPG).



Dimitrios Prousalis received the B.Sc. and M.Sc. degrees in physics, specializing in theoretical physics with strong interest in nonlinear dynamics and chaos, and the Ph.D. degree in theoretical physics from the Aristotle University of Thessaloniki, under the supervision Prof. Kyprianidis. During his Ph.D. degree, he focused on the dynamics of memristive systems and circuits. Following his Ph.D. degree, he joined as a Post-Doctoral Researcher with the Max Planck Institute for the Physics of Complex System, Dresden, Germany, to work on

emergent phenomena in networks of delay-coupled oscillators. His research interests include stochastic and chaotic dynamics of systems and circuits, particularly the synchronization of coupled oscillators and applying the theory of dynamical systems to engineering applications.



Jens Wagner was born in Freital, Germany, in 1981. He received the Dipl.-Ing. and Ph.D. degrees from the Chair for Circuit Design and Network Theory, Technische Universität Dresden (TU Dresden), in 2008 and 2017, respectively. Since 2010, he has been with the Chair of Circuit Design and Network Theory, TU Dresden. He is currently leading the RF Frontend Research Group, Chair for Circuit Design and Network Theory, and the Tactile Electronics Research Group, Centre for Tactile Internet with Human-in-the-Loop (CeTI), TU Dresden.



Frank Jülicher received the Ph.D. degree from the University of Cologne in 1994, under the supervision of Prof. Reinhard Lipowsky, and the Habilitation degree from the University of Paris VII in 2000. Following his post-doctoral research at Simon Fraser University, Canada, Institut Curie, Paris, and ESPCI, France, he was appointed as a CNRS Researcher at Institut Curie in 1998. Since 2002, he has been the Director of the Max Planck Institute for the Physics of Complex Systems, Dresden, Germany, and a Professor of biophysics with TU Dresden. His

major research interests include theoretical approaches to dynamic processes in cells and tissues, which include active cellular processes, such as cellular oscillations, cell division, and collective phenomena, including tissue morphogenesis. He received the Robert Wichard Pohl Prize of the DPG, the Raymond and Beverly Sackler International Prize in Biophysics, and the Gottfried Wilhelm Leibniz Prize.



Frank Ellinger (Senior Member, IEEE) was born in Friedrichshafen, Germany. He received the degree in electrical engineering (EE) from the University of Ulm, Germany, in 1996, the Diploma degree in business and administration and the Ph.D. degree in EE from ETH Zürich, Switzerland, in 2001, and the Venia Legendi (University Teaching) degree in high-frequency circuit design from ETH Zürich in 2004, for his habilitation thesis. He was a Lecturer of high-frequency circuit design with ETH Zürich from 2002 to 2006. From 2001 to 2006, he was

the Head of the RFIC Design Group, Electronics Laboratory, ETH Zürich, and a Project Leader with the IBM/ETH Competence Center for Advanced Silicon Electronics, IBM Research, Rüschlikon. Since August 2006, he has been a Full Professor and the Head of the Chair for Circuit Design and Network Theory, Technische Universität Dresden, Germany. He published more than 500 refereed scientific papers. His core expertise is in the area of integrated circuits for wireless and optical communications. He was the coordinator of the communication systems area of the BMBF cluster Cool Silicon and a member of the Management Board of the Cool Silicon e.V. He is the Coordinator of the BMBF Zwanzig20 Cluster Fast Actuators Sensors and Transceivers (FAST) with 90 partners and a Speaker of the DFG Priority Program FFlexCom. He is/was the Coordinator of several EU funded projects, such as DIMENSION, ADDAPT, RESOLUTION, MIMAX, and FLEXIBILITY. For his works, he received several awards, including the Vodafone Innovation Award, the Alcatel Lucent Science Award, the IEEE MTT-S Outstanding Young Engineer Award, the ETH Medal, the Denzler Award of the Swiss Federal Association of Electrical Engineers, the Rohde & Schwarz, Agilent twice, and the Gerotron EEEfCOM Innovation Award. He was an Organizer and the Chair of several conferences, such as the European Solid State Circuits Conference (ESSCIRC) in 2018. From 2005 to 2006, he served as an Associate Editor for the IEEE MICROWAVE AND WIRELESS COMPONENT LETTERS. He has been elected by the IEEE Microwave Theory and Techniques (MTT) Society as an IEEE Distinguished Microwave Lecturer.